Commun Nonlinear Sci Numer Simulat 18 (2013) 2549–2561

Contents lists available at SciVerse ScienceDirect

Commun Nonlinear Sci Numer Simulat

journal homepage: www.elsevier.com/locate/cnsns

Hysteresis phenomena in shape memory alloys by non-isothermal Ginzburg–Landau models

R.P. Dhote [a,c,*], M. Fabrizio [b], R.N.V. Melnik [c,d], J. Zu [a]

[a] Department of Mechanical and Industrial Engineering, University of Toronto, 5 King's College Road, Toronto, ON, Canada M5S-3G8
[b] Department of Mathematics, University of Bologna, Piazza di Porta S. Donato 5, I-40126 Bologna, Italy
[c] M²NeT Laboratory, Wilfrid Laurier University, 75 University Avenue, Waterloo, ON, Canada N2L-3C5
[d] Universidad Carlos III de Madrid, Avenida de la Universidad 30, Leganes E28911, Spain

ARTICLE INFO

Article history:
Received 21 August 2012
Received in revised form 24 January 2013
Accepted 24 January 2013
Available online 4 February 2013

Keywords:
Phase field model
Ginzburg–Landau theory
Nonlinear thermo-elasticity
Non-isothermal models

ABSTRACT

In this paper, we propose the new one- and three- dimensional models for the description of hysteretic phenomena in shape memory alloys (SMAs). These thermodynamic models are non-isothermal and allow to account for the thermo-mechanical material properties of both austenite and martensite phases based on the local phase value of the order parameter. They are based on the Ginzburg–Landau free energy and the phase field theory. The core of the models is a phase evolution governed by the time dependent Ginzburg–Landau (TDGL) equation and the conservation balance laws with nonlinear coupling between stress, strain and the phase order parameter. The models account for the gradient energy and have been tested in the study of material properties evolution under harmonic stress loading for all important practical cases. The representative numerical simulations have been carried out here without the gradient energy term. The developed models account for the phase dependent properties based on the compliance tensor as a function of the order parameter and stress. We also compared the results obtained with these models and observed differences in homogeneous and inhomogeneous situations due to the change in compliance. In this way, the description of quasiplastic and pseudoelastic behaviors in SMA specimens is improved and becomes in an agreement with existing experiments.

1. Introduction

There has been an increasing interest in studying SMA properties due to both theoretical challenges and practical applications. These properties include the ability of these materials to produce large strains, nonlinear hysteretic behaviors and recoverable (memory) shapes. They arise due to the underlying phenomenon caused by phase transformations. These transformations are due to an atomic reordering phenomenon caused by the displacement of atoms from a high symmetry arrangement (known as the austenite phase) to low symmetry arrangements (known as the martensite phases) with displacements less than an atomic distance. The atomic rearrangements can be induced by stress or temperature loadings. There is a finite number of atomic rearrangements from austenite to martensite variants in the sense of point group theory (for example, three tetragonal martensitic arrangements from the cubic austenite NiAl crystals, twelve monoclinic-I martensitic arrangements from the cubic austenite NiTi crystals, etc.). The martensitic phases (or variants) are accommodated

* Corresponding author at: Department of Mechanical and Industrial Engineering, University of Toronto, 5 King's College Road, Toronto, ON, Canada M5S-3G8. Tel.: +14169463709.
E-mail address: rakesh.dhote@mail.utoronto.ca (R.P. Dhote).

1007-5704/$ - see front matter © 2013 Elsevier B.V. All rights reserved.
http://dx.doi.org/10.1016/j.cnsns.2013.01.015

in different orientations to minimize the strain energy [1]. Although the transformation strain (or Bain strain) causing such transformations is small, the effects over large numbers of atomic crystals are added to get a macroscopic deformation in SMA samples. These atomic rearrangements cause temperature and stress hysteresis and give rise to two unique properties namely, the shape memory effect and superelasticity [2].

Although the first SMA material was discovered in 1932 (by Ölander in Au-Cd alloy [3]), up until today their mathematical modeling remains a challenging task in science and engineering. The main reasons behind that is the inherent nonlinear thermo-mechanical coupling and the austenite to martensite phase transformations. A number of different modeling approaches, developed over last few decades to capture SMA properties, have been extensively discussed in the literature [4–13].

While some of these approaches led to the development of efficient generic multiscale numerical procedures that can be applied to a wider class of models of nonlinear thermoelasticity [4,6], the others can be broadly classified as (a) micromechanical models [14,15] based on the microstructures and homogenization techniques, (b) phenomenological models [16] based on plasticity theory, and (c) phase field (PF) models [17–19] based on the first order kinetic TDGL theory. It is the latter group of models that are of particular interest in the present paper. The PF models have been widely used to study the solid-to-solid phase transformations [20,21] and SMAs at various length scales [22–28]. It is a unified framework that describes stress and temperature induced phase transformations. The research works based on PF models differ in the choice of order parameter (order parameter (OP) describes the different phases in a domain), thermodynamic potentials, model formulation, and numerical approaches [25,17,29,22,4,10].

Falk [30] proposed a free energy based on the Landau-Devonshire theory using higher-order polynomial potential with shear strain as an OP to describe the shape memory effect. Wang and Khachaturyan [31] modeled martensitic transformations taking into account transformations induced elastic strain OPs and time dependent Ginzburg–Landau (TDGL) equations. Curnoe and Jacobs [32], Lookman et al. [23], Bouville and Ahluwalia [24,33] used Landau theory using elastic strain components and their gradients to describe the dynamics of phase transformations. One of the previous notable works in the PF theory is the model developed by Levitas and Preston [17–19]. The major feature of the model is that it incorporates the material properties of both austenite and martensite phases based on the local phase value, and defines the different phase transformations between austenite and martensite variants. The number of phase evolution equations in a model equals the number of martenstic variants considered in a system. The elastic compliances are dependent on OPs are used in the model, at larger strains. Later, Mahapatra and Melnik [34,35] derived a non-isothermal model based on the free energy developed by Levitas and Preston [17–19] by modifying the multivariant framework to obtain strongly coupled thermo-mechanical models with essential properties of frame indifference and material symmetry. A series of computational results were reported for various dimensional reductions of the model (e.g. [13] and references therein). The PF models have also been used to study stress induced phase transformations properties under the influence of anisotropy and disorder [36], as well as studies of interface propagation and microstructure evolution in SMAs (e.g. [37,38] and references therein).

More recently, Berti et al. [29,39], Fabrizio [40,41], Grandi et al. [26], and Maraldi et al. [27] developed a non-isothermal thermodynamic framework for dealing with one dimensional and three dimensional phase transformations in SMAs. Their studies were based on a simplified version of the free energy developed by Levitas and Preston [17]. One of the important features of the 3D model within this framework is the use of a scalar phase OP instead of the tensorial phase OP [29]. The application of this approach reduces the problem size by limiting the evolution equation to one, instead of considering separate equations for each crystallographic variant as described in [17–19]. This results in simple and efficient implementation. The basic model within this framework is the first order phase kinetic TDGL evolution equation complemented by the conservation balance laws of momentum and energy transfer. In addition, the model contains appropriate constitutive equations coupling the stress, strain and phase order parameter. The model is consistent with the laws of thermodynamics. The above models describe the pseudoelastic and shape memory effects in SMAs under the assumption of equal elastic compliances of austenite and martensite phases. However, experimental results [2,3] demonstrate that this assumption cannot be justified as material properties are different for austenite and martensite phases. Note, for example, that the stiffness of austenite phase in NiTi is almost four times that of its martensite variants. Hence, it is very important to incorporate the material properties of austenite and martensite variants in this promising model, one of the tasks which we will undertake in the present paper.

In this paper, we modify the one dimensional and three dimensional PF models proposed in [39] to account for the material properties of both austenite and martensite phases by introducing a compliance tensor that depends on the material properties via the local phase OP and stress value. The one dimensional model is appropriate for describing properties of the typical SMA wire specimen, and the three dimensional model is used in a general sense. The dependence on phase and stress is essential in our newly developed models for capturing the realistic properties of SMAs. This leads to a set of tasks that have been completed in this contribution. First, the results obtained with the newly developed one dimensional model, that uses the modified compliance variable, have been compared with the homogeneous material properties (equal compliances) of both phases. Here, a point to be noted that the homogeneous and non-homogeneous material properties used during the simulations do not refer to the incorporation of domain wall (gradient energy term) as described in [25], but rather they correspond to the compliance of the material. All the numerical simulations have been carried out in this paper, using the stress loading of a SMA domain in the absence of gradient energy term. However, since the model accounts for gradient energy term explicitly, this can be extended in future. The one dimensional non-isothermal model, with equal compliances of both phases, has been used to study the SMA response to stress- and strain- induced loadings by incorporat-

ing the gradient energy [27,26]. Next, a new generalized 3D model for austenite–martensite phase transformations has also been proposed and its consistency with the laws of thermodynamics has been discussed. Finally, we carry out the numerical simulations for simplified pseudo-2D specimens and compare the results with the one dimensional model. We demonstrate that the models capture typical SMA properties using the dimensionless material properties. The model is implemented to capture the SMA properties of NiTi specimen in [26,27].

Based on the above tasks, the paper is organized as follows. In Section 2, a one dimensional model and numerical simulations are discussed in different practically important cases. The key feature of this model is its ability to account for the properties of both austenite and martensite phases by incorporating the stress and order parameter dependent compliance variable. The generalized three dimensional model is presented in Section 3 where we also discuss the thermodynamic consistency of the model, carry out numerical experiments and compare the models. Conclusions are given in Section 4.

2. One dimensional model

We develop the one dimensional model to study the response of the SMA wire specimen, which find wide practical applications. We start from a new model of the Gibb's free energy function, accounting for the compliance tensor to accommodate nonlinear thermo-mechanical properties of both phases. Then, we move to a one-dimensional model developed in [39] (see also [29,40,41]) and modify it to incorporate the material properties of both austenite and martensite variants depending on the local phase (ϕ) and stress values. The resulting model can deal with the austenite phase ($\phi = 0$) and two martensite variants M± denoted by $\phi = \pm 1$. We demonstrate the basic capabilities of the developed model on a series of numerical examples, covering all most important practical cases.

2.1. Mathematical model

The model is developed with Gibb's free energy functional $\mathscr{G}$ to describe austenite–martensite phase transformations by using the 2-4-6 order polynomial potentials. In particular, we generalize the model considered in [39] by means of the free energy function having the following form:

$$\mathscr{G}(\theta,\sigma,\phi,\nabla\phi) = \mathscr{G}_0(\theta) - \frac{1}{2}\lambda(\sigma,\phi)\sigma^2 + \frac{\kappa}{2}\mid\nabla\phi\mid^2 + \theta_0 F(\phi) + [\hat{\theta} - \epsilon_0\sigma sign(\phi)]G(\phi), \tag{1}$$

where $\mathscr{G}_0$ represents the thermally dependent part (being a function of the absolute temperature θ),$\kappa, \theta_0, \epsilon_0$ are constants, the potentials $F(\phi)$ and $G(\phi)$ are defined as

$$F(\phi) = \frac{1}{6}\phi^6 - \frac{1}{2}\phi^4 + \frac{1}{2}\phi^2, \quad G(\phi) = \begin{cases} \frac{1}{4} & \text{if } |\phi| \geqslant 1, \\ -\frac{1}{4}\phi^4 + \frac{1}{2}\phi^2, & \text{if } |\phi| < 1, \end{cases} \tag{2}$$

and

$$\hat{\theta} = max\{\alpha(\theta - \theta_A), \alpha(\theta_0 - \theta_A)\}, \quad \alpha > 0, \quad \theta_A > \theta_0. \tag{3}$$

The temperature θ_M is defined in relation with temperatures θ_0, θ_A, and the slope α of the $\sigma\epsilon_0 - \theta$ space as $\theta_0 = \alpha(\theta_A - \theta_M)$.

In the works of Berti et al. [29,39] and Fabrizio [40,41], the equal elastic compliances of austenite and martensite phases are assumed in the model. As stated earlier, the elastic compliances of austenite and martensite phases of SMA materials could be different, hence it is important to incorporate the different elastic compliances for each phase. In this work, we modify the compliance tensor λ in Eq. (1) to accommodate the thermo-mechanical properties of austenite and martensite phases based on the OP value and stress [17]. It is defined as

$$\lambda(\sigma,\phi) = \lambda_2(\phi) + \lambda_3(\phi)\sigma + \lambda_4(\phi)\sigma\cdot\sigma, \tag{4}$$

where $\lambda_2, \lambda_3, \lambda_4$ are the tensor of 4^{th} , 6^{th}, and 8^{th} order, respectively.

The phase diagram $\sigma\epsilon_0 - \theta$ can be obtained with the procedure outlined in [39]. The plots of the free energy potentials F(ϕ), G(ϕ) and phase diagram are shown in Fig. 1(a) and (b) respectively. The temperatures $\theta_0, \theta_M, \theta_A$ are adjustable parameters ($\theta_0 < \theta_M < \theta_A$) used to tune the phase diagram. It should be noted that θ_M refers to the average temperature of martensite start (M_s) and martensite finish (M_f) temperature, and θ_A refers to the average temperature of austenite start (A_s) and austenite finish (A_f) temperature.

The phase evolution in SMA is governed by the first-order kinetic TDGL equation as

$$\gamma\frac{\partial\phi}{\partial t} = -\frac{\partial\mathscr{G}}{\partial\phi} + \nabla\cdot\left(\frac{\partial\mathscr{G}}{\partial(\nabla\phi)}\right). \tag{5}$$

On substituting Eq. (1) in Eq. (5), we obtain

$$\gamma\frac{\partial\phi}{\partial t} = \kappa\frac{\partial^2\phi}{\partial x^2} - \theta_0\left[\frac{\partial}{\partial\phi}F(\phi) + \beta[\phi + sign(\sigma)]\right] - [\hat{\theta} - \epsilon_0\sigma sign(\phi)]\frac{\partial}{\partial\phi}G(\phi), \tag{6}$$

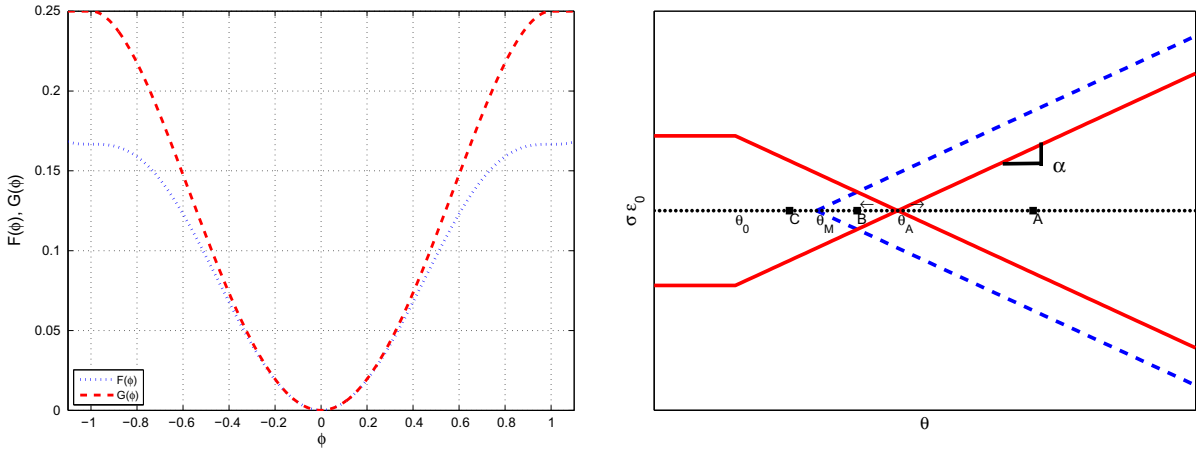

(a) Free energy potentials F(ϕ) and G(ϕ)

(b) Phase diagram $\sigma\epsilon_0 - \theta$ space

Fig. 1. Free energy potentials and $\sigma\epsilon_0 - \theta$ space for one dimensional model.

where β is introduced as a small perturbing term ($0 < \beta \ll 1$) incorporated to prevent the arrest of ϕ value at $\phi = 0$ and $\phi = \pm 1$ as described in [39]. This is complemented with a suitable constitutive equation that couples the stress, strain, and OP ϕ in the domain. We define the constitutive equation in the one dimensional case, considered in this section, as

$$\epsilon = \lambda(\sigma, \phi)\sigma + \epsilon_0 sign(\phi) G(\phi). \tag{7}$$

The strain in Eq. (7) is decomposed into the elastic and phase transformation strains [17,29]. The elastic strain is related to the stress via phase dependent compliance. The transformation strain is related to the potential G as a function of local phase value.

2.2. Numerical experiments

Numerical methodologies for phase field and coupled thermo-mechanical models describing SMA dynamics have been developed extensively in recent years. Both finite element [42,34,35] and finite difference techniques [25,43] were applied. In the latter case, fully conservative numerical approximations were also developed [44] including various spectral and low-dimensional approximations [8,45,13]. Finally, an efficient method based on finite volume approximation was reported in [46]. In what follows, all numerical experiments in the 1D case have been carried out using the Matlab ODE solver. We solve the phase evolution equation Eq. (6) and then calculate the material response using Eq. (7). The transformation response is calculated at a single material point.

The simulations were performed for the following dimensionless material parameters:

$$\gamma = \frac{1}{100}, \quad \theta_0 = 1, \quad \theta_M = 2, \quad \theta_A = 3, \quad \epsilon_0 = 30, \quad \sigma_0 = 3, \quad \beta = \frac{1}{1000}, \quad E = 1, \quad k = 1 \quad \text{and} \quad \alpha = 1.$$

The mechanical properties and phase evolution have been studied in the absence of gradient energy term ($\kappa = 0$). The simulations have been carried out under three cases with different initial conditions of SMA wire in the austenite, intermediate, and martensite phase. We simulate the above three cases under two different scenarios. Firstly, we consider a situation where the material parameters are homogeneous for both austenite and martensite (equal elastic compliances), and secondly, we consider the situation with the material parameters of martensite is different from austenite (different elastic compliances) and dependent on the phase and stress value. We hereby refer these scenarios as linear λ, and nonlinear λ scenarios, respectively. The compliance tensor in the linear λ case is $\lambda_2 = E, \lambda_3 = 0$ and $\lambda_4 = 0$, and in the nonlinear λ case is $\lambda_2 = E + \frac{1}{10}E\phi^2, \lambda_3 = 0$, and $\lambda_4 = \frac{1}{10}E\phi^4$.

2.2.1. Case 1: Austenite phase ($\theta(20) > \theta_A(3)$)

This case refers to the point A in Fig. 1(b). Fig. 2(a) and (b) show the phase evolution and material behavior ($\sigma - \epsilon$ curve) for linear λ and nonlinear λ scenarios. The phase evolution ϕ for both scenarios follows the same trend as it is governed by the harmonic stress $\sigma = \sigma_0 \sin(kt)$. It is observed from Fig. 2(a) that austenite phase ($\phi = 0$) switches to the martensite variant $\phi = 1$ after it crosses a critical stress value at the particular temperature. The stress–strain curve behaves elastically along the path o-a-b for linear λ scenario. The phase change from austenite to favored martensite variant ($A \rightarrow M+$) occurs along the path b-c at constant stress and elastic loading resumes along the path c-d. During the positive unloading part of the sinusoidal cycle, the elastic unloading occurs along the path d-c-e. The martensite transformation to austenite ($M+ \rightarrow A$) occurs when the stress level falls below the critical stress value. The specimen is unloaded to zero stress–strain state by elastic

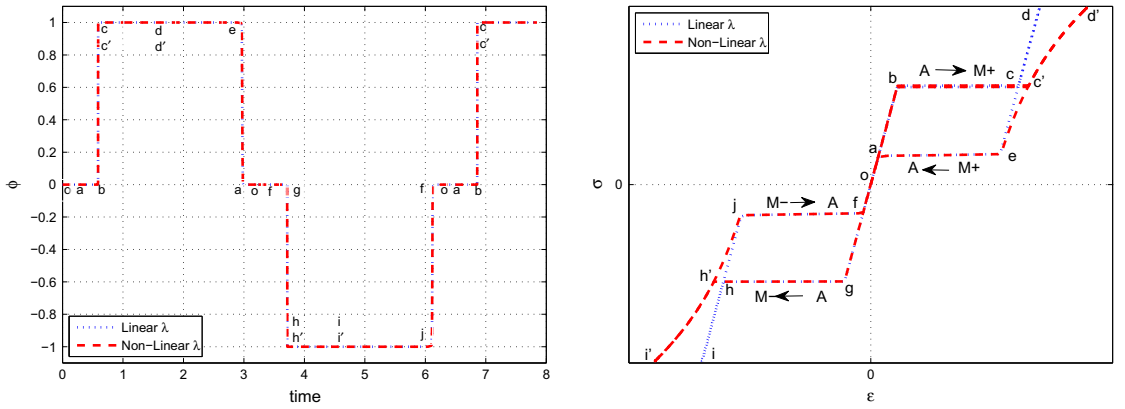

(a) ϕ vs time (b) $\sigma - \epsilon$ curve

Fig. 2. Case 1: Material response of a SMA specimen at $\theta(20) > \theta_A(3)$.

unloading along the path a-o. The phase transformations $A \rightarrow M+$ and $M+ \rightarrow A$ take place at the positive stress value creating the pseudoelastic response. In the negative part of the sinusoidal cycle, the $M-$ variant of martensite is favored and σ-ϵ curve follows the path o-f-g-h-i-j-f-o.

For the nonlinear λ scenario, the σ–ϵ curve behaves in the same way as during the elastic loading along the path o-a-b, however the difference is observed during the phase transformation ($A \rightarrow M+$) which follows the path b-c′. The elastic loading of $M+$ phase resumes along the path c′-d′ following the unloading along the path d′-c′-e-a-o. The σ-ϵ curve follows the path along o-f-g-h′-i′-h′-j-f-o during the negative part of the sinusoidal cycle.

The deviation of σ-ϵ curve in the nonlinear λ from the linear λ happens due to the increase in compliance of martensitic phase as per Eq. (4) (i.e. the decrease in stiffness of the martensitic phase). The deviation of the σ-ϵ curve causes the increase in the area of stress hysteresis, leading to more energy dissipation. The decrease in the stiffness of martensite phase is attributed to the atomic arrangements where the nonsymmetric atomic structure can be easily distorted as compared to the regular symmetric atomic arrangements (where such a distortion requires higher energy).

2.2.2. Case 2: Intermediate phase ($\theta_M(2) < \theta(2.5) < \theta_A(3)$)

This case refers to the point B in Fig. 1(b). We have considered two subcases here depending upon the initial phase in material.

Subcase 1: SMA specimen initially at austenite phase $\phi(0) = 0$.

The phase evolution and σ–ϵ curve at the intermediate temperature with SMA specimen initially at austenitic state ($\phi = 0$) is shown in Fig. 3(a) and (b) respectively. One difference is observed that the $M+ \rightarrow A$ transformation takes place at the negative value of stress. This is because the phase transformation lags the stress cycle during the unloading. Hence it creates the hysteresis loop along the path o-a-b-c-d-e-f-g-h-i-j-a for the linear λ case and along the path o-a-b-c′-d′-e-f-g-h′-i′-j-a for the nonlinear λ case.

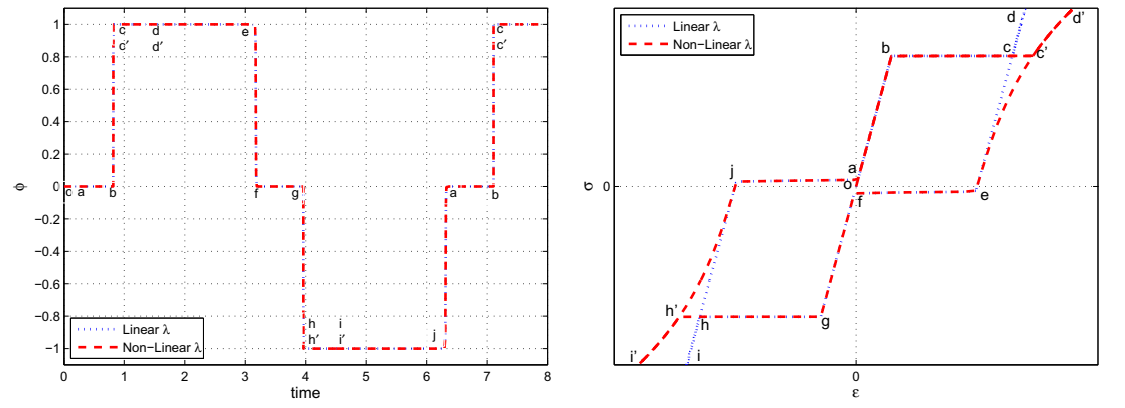

(a) ϕ vs time (b) $\sigma - \epsilon$ curve

Fig. 3. Case 2: Material response of a SMA specimen at intermediate temperature ($\theta_M(2) < \theta(2.5) < \theta_A(3)$) with initial phase as austenite ($\phi = 0$).

A point of observation that once deformed the curve does not return to the zero strain state. The separation between points *a* and *f* is small and depends on the temperature. Thus at the intermediate temperature, the σ–ϵ curve behaves like semi-quasiplastic material.

Subcase 2: SMA specimen initially at martensite phase $\phi(0) = 1$.

The phase evolution and the σ–ϵ curve at the intermediate temperature with SMA specimen initially at martensite state ($\phi = 1$) are shown in Fig. 4(a) and (b) respectively. As the material is initially in the martensite state, the elastic loading in $\sigma - \epsilon$ curve does not start from zero stress, rather it starts from point a. The material response (σ–ϵ curve) is similar to Fig. 3(b). The material behavior for the linear λ and the nonlinear λ cases as shown along a-b-c-d-e-f-g-h-i-j-a and a-b-c′-d′-e-f-g-h′-i′-j-a paths, respectively.

2.2.3. Case 3: Martensitic phase ($\theta(1) < \theta_M(2)$)

This case refers to the point C in Fig. 1(b). In this case, the simulations were performed with the same dimensionless material parameters with the following modifications:

$$\gamma = \frac{1}{10}, \quad \epsilon_0 = 100, \quad \sigma_0 = 30, \quad \lambda_2 = E + \frac{1}{10}E\phi^2, \quad \lambda_4 = \frac{1}{1000}E\phi^4 \text{during the nonlinear } \lambda \text{ simulations.}$$

The phase evolution and σ–ϵ curve at the martensite state are shown in Fig. 5(a) and (b), respectively. The quasiplastic response of the material at lower temperature is observed. The bigger hysteresis loops, indicated by the path o-a-b-c-d-e-f-g-h-i-j-a for the linear λ case and indicated by the path o-a-b-c′-d′-e-f-g-h′-i′-j-a for the nonlinear λ case, are formed. The stress jumps from a-b and f-g are observed due to small elastic loadings during switching between martensite variants from $M- \rightarrow M+$ and $M+ \rightarrow M-$ respectively.

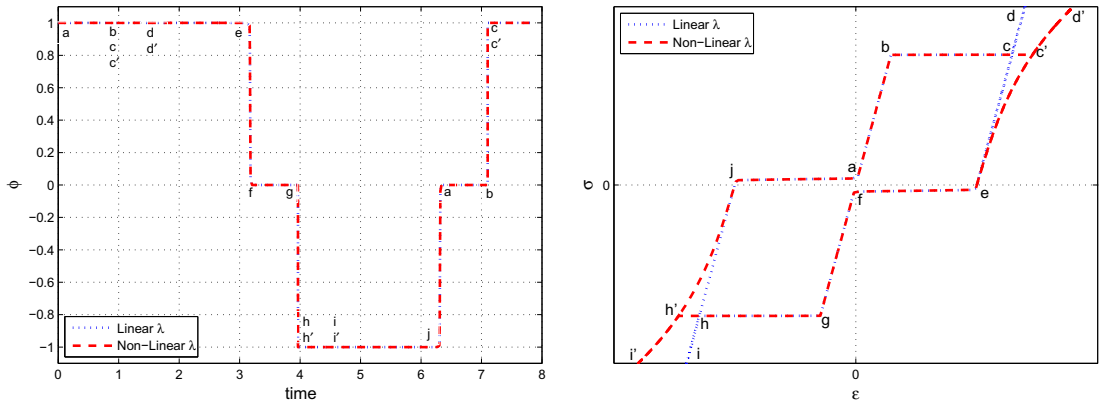

(a) ϕ vs time (b) $\sigma - \epsilon$ Curve

Fig. 4. Case 2: Material response of a SMA specimen at intermediate temperature ($\theta_M(2) < \theta(2.5) < \theta_A(3)$) with initial phase as martensite variant ($\phi = 1$).

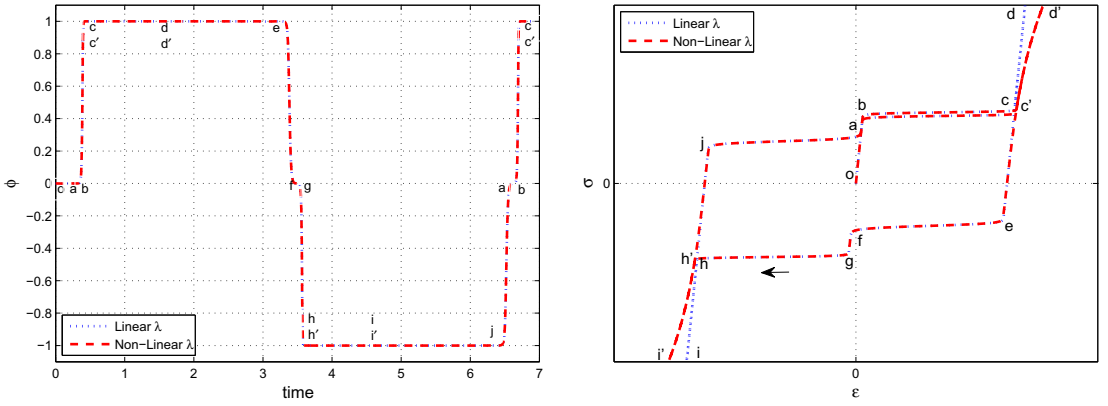

(a) ϕ vs time (b) $\sigma - \epsilon$ Curve

Fig. 5. Case 3: Material response of a SMA specimen below martensitic temperature $\theta(1) < \theta_M(2)$.

Thus, the one dimensional model captures the essential SMA properties of pseudoelasticity, semi-quasiplasticity, and quasiplasticity at higher, intermediate, and lower temperatures, respectively.

3. Three dimensional model

In this section, we develop a generalized three dimensional model for the description of SMA dynamics. The model is developed with free energy potentials based on 2-3-4 polynomials. Unlike the one dimensional model considered in the previous section, this model describes the austenite–martensite transformation with no distinction between martensite variants. In contrast to the multivariant models developed in [17–19,34,35], where each martensitic variant is described by a separate phase evolution equation, this model has a simplified representation with scalar order parameter from the interval $[0,1]$ with $\phi = 0$ being the austenite and $\phi = 1$ being the martensite phase. This lead to a simpler model of PTs and thermomechanical dynamics with only one order parameter, which is computationally tractable, but at the expense of distinction of two martentic variants phases individually. Similar to Section 2, we incorporate the material properties of both austenite and martensite phases based on the compliance tensor. The numerical simulations to study a few illustrative one dimensional and quasi-2D specimens have been carried out and the results are discussed below.

The model describes the evolution of scalar OP based on the TDGL equation. The first order kinetic TDGL equation is complemented with conservation laws of momentum and energy transfer. The developed model for SMA evolution is strongly coupled with structural, thermal, and phase evolution equations.

3.1. Mathematical model

The model consists of structural and thermal parts complemented with the appropriate constitutive equations coupling stress, strain and phase evolution order parameter. We start with the structural part of the model. The balance equation is given by the conservation law of momentum. It reads as

$$\rho_0 \ddot{\boldsymbol{u}} = \nabla \cdot \boldsymbol{\sigma} + \rho_0 \boldsymbol{f}, \tag{8}$$

where ρ_0 is the density, $\boldsymbol{u}$ is the displacement, $\boldsymbol{\sigma}$ is the stress tensor, $\boldsymbol{f}$ is the body force. The strain tensor $\boldsymbol{\epsilon}$ is defined as

$$\boldsymbol{\epsilon} = \frac{1}{2}[\nabla \boldsymbol{u} + \nabla \boldsymbol{u}^T]. \tag{9}$$

We choose the 2-3-4 polynomials free energy having minimas at $\phi = 0$, and $\phi = 1$ with no distinction of martensitic variants. The free energy based Ginzburg–Landau potential is given as

$$\Phi = \frac{\kappa}{2}|\nabla \phi|^2 - \frac{1}{2}(\boldsymbol{\sigma}\boldsymbol{\lambda} \cdot \boldsymbol{\sigma}) + \theta_0 F(\phi) + (\hat{\theta} - \epsilon_0 \frac{\boldsymbol{\sigma} \cdot \boldsymbol{\sigma}}{|\boldsymbol{\sigma}|}) G(\phi). \tag{10}$$

The phase evolution in SMA can be described by the first-order kinetic TDGL equation as follows:

$$\gamma \frac{\partial \phi}{\partial t} = \kappa \Delta \phi - \theta_0 \frac{\partial F(\phi)}{\partial \phi} - \left(\hat{\theta} - \epsilon_0 \frac{\boldsymbol{\sigma} \cdot \boldsymbol{\sigma}}{|\boldsymbol{\sigma}|}\right) \frac{\partial G(\phi)}{\partial \phi}, \tag{11}$$

where γ and θ_0 are constants and the potentials $F(\phi)$ and $G(\phi)$ are defined as

$$F(\phi) = \frac{1}{4}\phi^4 - \frac{2}{3}\phi^3 + \frac{1}{2}\phi^2 + \beta(\phi^2 - \phi), \quad G(\phi) = \begin{cases} 0 & \text{if } \phi < 0, \\ -\frac{1}{4}\phi^4 + \frac{1}{2}\phi^2 & \text{if } 0 \leqslant \phi \leqslant 1, \\ \frac{1}{4} & \text{if } \phi > 1, \end{cases} \tag{12}$$

the constant β is the perturbing term added to accommodate slope variations in the regime of instability ($0 < \beta \ll 1$) as described in [39]. Finally

$$\hat{\theta} = \begin{cases} \theta - \theta_A & \text{if } \theta > \theta_A, \\ 0 & \text{if } \theta \leqslant \theta_A, \end{cases} \tag{13}$$

where $\theta_A > \theta_0$. The temperature θ_M is defined as $\theta_M = \theta_A - \theta_0$.

The free energy potentials $F(\phi)$ and $G(\phi)$ and the phase space diagram $|\boldsymbol{\sigma}|\epsilon_0 - \theta$ are plotted in Fig. 6(a) and (b), respectively.

The definition of the structural model (excluding the thermal part) is completed by defining the suitable constitutive equation coupling the $\boldsymbol{\sigma}$, $\boldsymbol{\epsilon}$, and ϕ. To account different forms of dependencies of compliance on ϕ and $\boldsymbol{\sigma}$, we define the constitutive equation as rate of change of strain, stress and ϕ parameters as follows

$$\dot{\boldsymbol{\epsilon}} = \boldsymbol{\lambda}^{1/2}(\boldsymbol{\sigma}, \phi) \frac{\partial}{\partial t}(\boldsymbol{\lambda}^{1/2}(\boldsymbol{\sigma}, \phi)\boldsymbol{\sigma}) + \epsilon_0 \frac{\boldsymbol{\sigma}}{|\boldsymbol{\sigma}|} \dot{G}(\phi). \tag{14}$$

The $\boldsymbol{\lambda}$ in Eq. (14) is the compliance tensor added to accommodate the thermo-mechanical properties of both austenite and martensite phases based on the OP value and stress [17]. In the general 3D case, it is defined as

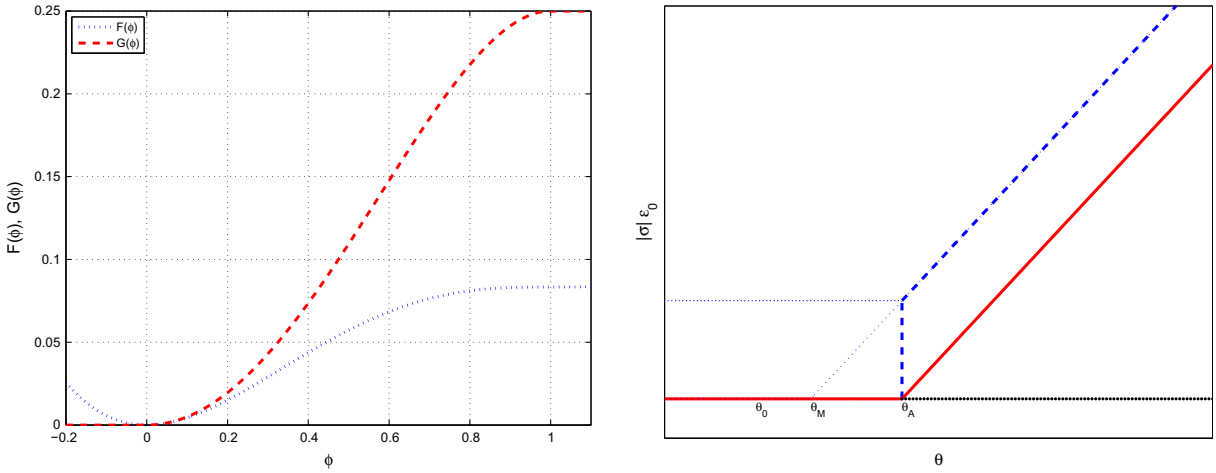

(a) Free energy potentials F(ϕ) and G(ϕ)

(b) Phase space diagram $|\sigma|\epsilon_0 - \theta$

Fig. 6. Free energy potentials and phase space diagram $|\boldsymbol{\sigma}|\epsilon_0 - \theta$ for the three dimensional model.

$$\boldsymbol{\lambda}(\boldsymbol{\sigma},\phi) = \boldsymbol{\lambda}_2(\phi) + \boldsymbol{\lambda}_3(\phi)\boldsymbol{\sigma} + \boldsymbol{\lambda}_4(\phi)\boldsymbol{\sigma}\cdot\boldsymbol{\sigma}, \tag{15}$$

where $\boldsymbol{\lambda}_2$, $\boldsymbol{\lambda}_3$, $\boldsymbol{\lambda}_4$ are the tensor of $4^{th}, 6^{th}$, and 8^{th} order, respectively.

Now the structural field model and the phase evolution model can be complemented with the thermal field model. The governing equation of the thermal field is now defined by the first law of thermodynamics as

$$\rho_0\dot{e}(\boldsymbol{\sigma},\phi,\theta) = \mathscr{P}^i_m + \mathscr{P}^i_\phi + \mathscr{P}^i_h, \tag{16}$$

where e denotes the internal energy, $\mathscr{P}^i_m$ is the internal mechanical power, $\mathscr{P}^i_\phi$ is the internal order structure power, and $\mathscr{P}^i_h$ is the internal heat power. They are defined as

$$\begin{aligned}
\mathscr{P}^i_m &= \boldsymbol{\sigma}\cdot\dot{\boldsymbol{\epsilon}},\\
\mathscr{P}^i_\phi &= \gamma\dot{\phi}^2 + \frac{\kappa}{2}\frac{d}{dt}(|\nabla\phi|^2) + \theta_0\dot{F}(\phi) + \left(\hat{\theta} - \epsilon_0\frac{\boldsymbol{\sigma}\cdot\boldsymbol{\sigma}}{|\boldsymbol{\sigma}|}\right)\dot{G}(\phi),\\
\mathscr{P}^i_h &= \rho_0 h,
\end{aligned} \tag{17}$$

where h is the rate at which heat is absorbed per unit mass. The $\mathscr{P}^i_\phi$ is obtained by multiplying Eq. (11) by $\dot{\phi}$ and following the approach in [29,40,41]. (The Frobenius inner product of two second rank tensors $\mathbf{A}$ and $\mathbf{B}$ is defined as $\mathbf{A}\cdot\mathbf{B} = \sum_i\sum_j A_{ij}B_{ij}$.)

By using Eq. (14), the $\mathscr{P}^i_m$ can now be written as

$$\mathscr{P}^i_m = \boldsymbol{\sigma}\cdot\dot{\boldsymbol{\epsilon}} = \frac{1}{2}\frac{d}{dt}(\boldsymbol{\lambda}(\boldsymbol{\sigma},\phi)\boldsymbol{\sigma}\cdot\boldsymbol{\sigma}) + \epsilon_0\frac{\boldsymbol{\sigma}\cdot\boldsymbol{\sigma}}{|\boldsymbol{\sigma}|}\dot{G}(\phi). \tag{18}$$

Assuming the Fourier constitutive law for the heat flux (see [4,5] for the models based on the Cattaneo-Vernotte relationship), the energy balance equation is written as ($\rho_0 = 1$)

$$h = -\nabla\cdot\boldsymbol{q} + r, \tag{19}$$

where $\boldsymbol{q}$ is the heat flux, r is the heat supply, and the heat flux is $\boldsymbol{q} = -k(\theta)\nabla\theta$, with $k(\theta) > 0$.

Now, we prove consistency of the above model with the second law of thermodynamics. By using the Clausius–Duhem inequality, we have

$$\dot{\eta} \geqslant -\nabla\cdot\left(\frac{\boldsymbol{q}}{\theta}\right) + \frac{r}{\theta}. \tag{20}$$

Using Eqs. (16), (17) and (19), the inequality yields

$$\theta\dot{\eta} \geqslant \frac{\boldsymbol{q}}{\theta}\cdot\nabla\theta + \dot{e} - \mathscr{P}^i_m - \mathscr{P}^i_\phi. \tag{21}$$

The free energy ψ is defined in the terms of internal energy e and entropy η as

$$\psi = e - \theta\eta. \tag{22}$$

Now, the inequality Eq. (21) is reduced to

$$\dot{\psi} + \dot{\theta}\eta - \mathscr{P}^{i}_{m} - \mathscr{P}^{i}_{\phi} + \frac{\boldsymbol{q}}{\theta}\cdot\nabla\theta \leqslant 0. \tag{23}$$

Substituting Eqs. (17) and (18), the last inequality is reduced to

$$\dot{\psi} + \dot{\theta}\eta \leqslant -\frac{\boldsymbol{q}}{\theta}\cdot\nabla\theta + \frac{1}{2}\frac{d}{dt}(\boldsymbol{\lambda}(\boldsymbol{\sigma},\phi)\boldsymbol{\sigma}\cdot\boldsymbol{\sigma}) + \gamma\dot{\phi}^2 + \kappa\nabla\phi\cdot\nabla\dot{\phi} + \theta_0\dot{F}(\phi) + \hat{\theta}\dot{G}(\phi). \tag{24}$$

We assume that the free energy ψ depends on the variables $\phi, \nabla\phi, \boldsymbol{\sigma}, \theta$, so that Eq. (24) can be written as

$$\left(\eta + \frac{\partial\psi}{\partial\theta}\right)\dot{\theta} + \left(\frac{\partial\psi}{\partial\phi} - \theta_0 F'(\phi) - \hat{\theta}G'(\phi)\right)\dot{\phi} + \left(\frac{\partial\psi}{\partial\nabla\phi} - \kappa\nabla\phi\right)\cdot\nabla\dot{\phi} + \left(\frac{\partial\psi}{\partial\boldsymbol{\sigma}} - \boldsymbol{\lambda}(\boldsymbol{\sigma},\phi)\boldsymbol{\sigma}\right)\cdot\dot{\boldsymbol{\sigma}} - \gamma\dot{\phi}^2 + \frac{\boldsymbol{q}}{\theta}\cdot\nabla\theta \leqslant 0. \tag{25}$$

Usual arguments of thermodynamics based on the arbitrariness of $\dot{\phi}, \nabla\dot{\phi}, \dot{\boldsymbol{\sigma}}, \dot{\theta}$ allow to prove that Eq. (25) implies the relations

$$\eta = -\frac{\partial\psi}{\partial\theta}, \quad \frac{\partial\psi}{\partial\phi} = \theta_0 F'(\phi) + \hat{\theta}G'(\phi), \quad \frac{\partial\psi}{\partial\nabla\phi} = \kappa\nabla\phi, \quad \frac{\partial\psi}{\partial\boldsymbol{\sigma}} = \boldsymbol{\lambda}(\boldsymbol{\sigma},\phi)\boldsymbol{\sigma}, \tag{26}$$

where F' and G' are derivatives with respective to OP ϕ.

Substituting Eq. (26) in Eq. (25) leads to

$$\frac{k(\theta)}{\theta}|\nabla\theta|^2 + \gamma\dot{\phi}^2 \geqslant 0, \tag{27}$$

thus the thermodyamic consistency follows from the positivity of the thermal conductivity k.

The relations in Eq. (26) enforce the following representation of the free energy:

$$\psi = \psi_0(\theta) + \frac{1}{2}(\boldsymbol{\lambda}(\boldsymbol{\sigma},\phi)\boldsymbol{\sigma}\cdot\boldsymbol{\sigma}) + \frac{\kappa}{2}|\nabla\phi|^2 + \theta_0 F(\phi) + \hat{\theta}G(\phi). \tag{28}$$

Using Eqs. (26)–(28), we obtain the expression of the entropy as

$$\eta = -\frac{\partial\psi}{\partial\theta} = -\psi_0'(\theta) - \hat{\theta}'G(\phi), \tag{29}$$

where ψ_0' and $\hat{\theta}'$ are the derivatives with respect to temperature θ.

Next, the internal energy can be simplified as

$$e = \psi + \theta\eta = e_0(\theta) + \frac{1}{2}(\boldsymbol{\lambda}(\boldsymbol{\sigma},\phi)\boldsymbol{\sigma}\cdot\boldsymbol{\sigma}) + \frac{\kappa}{2}|\nabla\phi|^2 + \theta_0 F(\phi) + (\hat{\theta} - \theta\hat{\theta}')G(\phi), \tag{30}$$

where $e_0 = \psi_0 - \theta\psi_0'$.

On differentiating Eq. (30) with respect to time and equating to the right hand side of Eq. (16), we obtain the heat equation as

$$\dot{e}_0(\theta) - \theta[G(\phi)\hat{\theta}''\dot{\theta} + \hat{\theta}'\dot{G}(\phi)] - \gamma\dot{\phi}^2 = -\nabla\cdot\boldsymbol{q} + r. \tag{31}$$

3.2. Numerical experiments

This section provides details of numerical experiments based on the newly developed three dimensional model. The phase evolution and stress–strain properties are studied for simplified 1D and pseudo-2D specimens. The results for pseudo-2D specimen are compared with numerical simulation results obtained with the one dimensional model from Section 2. Here, we only solve the phase transformation kinetic equation and structural constitutive equation to demonstrate the concept.

3.2.1. Simplified one dimensional specimen

For this case, the Eq. (11) is reduced to

$$\gamma\frac{\partial\phi}{\partial t} = \kappa\frac{\partial^2\phi}{\partial x^2} - \theta_0\frac{\partial}{\partial\phi}F(\phi) - [\hat{\theta} - \epsilon_0 \mid \boldsymbol{\sigma} \mid]\frac{\partial}{\partial\phi}G(\phi). \tag{32}$$

The numerical simulations have been carried out by using Eqs. (14) and (32) with the sinusoidal stress input $\sigma = \sigma_0\sin(kt)$ in the finite element software Comsol Multiphysics. The dimensionless material parameters used for the simulations were as follows:

$\gamma = \frac{1}{100}$, $\kappa = 0$, $\theta_0 = 1$, $\theta_M = 2$, $\theta_A = 3$, $\epsilon_0 = 30$, $\sigma_0 = 6$, $\beta = \frac{1}{1000}$, $E = 1$, and $\theta = 5$.

The stress tensor components in the one dimensional case are reduced for the linear $\boldsymbol{\lambda}$ case to $\boldsymbol{\lambda}_2 = E$, $\boldsymbol{\lambda}_3 = 0$ and $\boldsymbol{\lambda}_4 = 0$, and for the nonlinear $\boldsymbol{\lambda}$ case to $\boldsymbol{\lambda}_2 = E + \frac{1}{10}E\phi^2$, $\boldsymbol{\lambda}_3 = 0$, and $\boldsymbol{\lambda}_4 = \frac{1}{100}E\phi^4$.

The phase evolution and σ–ϵ curve of SMA specimen are shown in Fig. 7(a) and (b), respectively. The ϕ evolves from initial austenite phase ($\phi = 0$) to the martensite phase ($\phi = 1$). There is no distinction of martensitic variants at $\phi = 1$. The figure

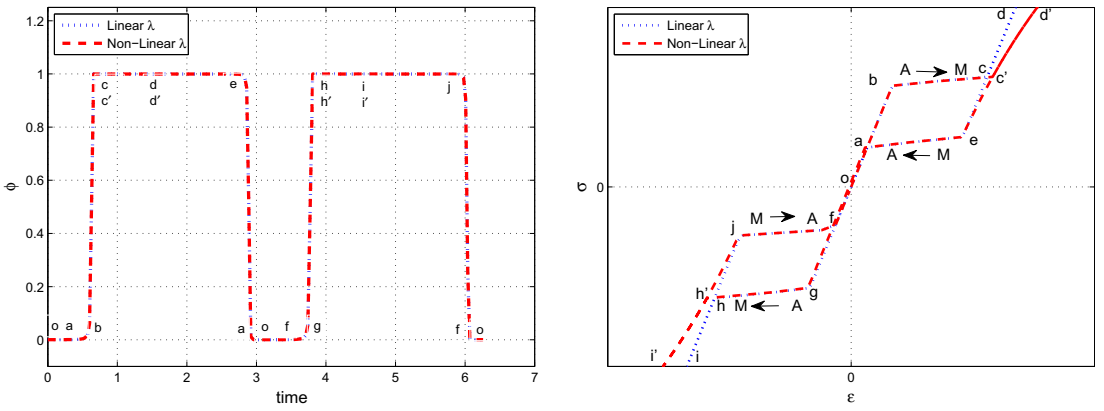

(a) ϕ vs time (b) $\sigma-\epsilon$ curve

Fig. 7. Material response of a SMA specimen at $\theta(5) > \theta_A(3)$.

captures the pseudoelastic σ–ϵ response and the stress hysteresis. The hysteresis loop followed during the harmonic loading is represented by the path o-a-b-c-d-e-a-o-f-g-h-i-j-f-o for the linear $\boldsymbol{\lambda}$ case and by the path o-a-b-c′-d′-e-a-o-f-g-h′-i′-j-f-o for the nonlinear $\boldsymbol{\lambda}$ case, respectively.

3.2.2. Quasi-2D model

The three dimensional model is now applied to the following quite illustrative quasi-2D case. The stress $\boldsymbol{\sigma}$ and strain $\boldsymbol{\epsilon}$ tensors are defined as

$$\boldsymbol{\sigma} = \begin{bmatrix} \sigma_{11} & 0 \\ 0 & \sigma_{22} \end{bmatrix} = A\sin(kt)\begin{bmatrix} \sigma_1 \sin^2(t+\vartheta) & 0 \\ 0 & \sigma_1 \cos^2(t+\vartheta) \end{bmatrix}, \tag{33}$$

$$\boldsymbol{\epsilon} = \begin{bmatrix} \epsilon_{11} & 0 \\ 0 & \epsilon_{22} \end{bmatrix} = B(t)\begin{bmatrix} g_1(t) & 0 \\ 0 & g_2(t) \end{bmatrix}, \tag{34}$$

with the additional condition

$$g_1(t) + g_2(t) = 1, \tag{35}$$

where A, k and ϑ are constants.

The rate dependent constitutive equation can be defined to establish a relationship between $\boldsymbol{\sigma}, \boldsymbol{\epsilon}$ and ϕ as

$$\frac{\partial \boldsymbol{\epsilon}}{\partial t} = \boldsymbol{\lambda}\frac{\partial \boldsymbol{\sigma}}{\partial t} + \epsilon_0 sign(\phi)\frac{\partial}{\partial t}G(\phi), \tag{36}$$

while the phase evolution equation can be written as

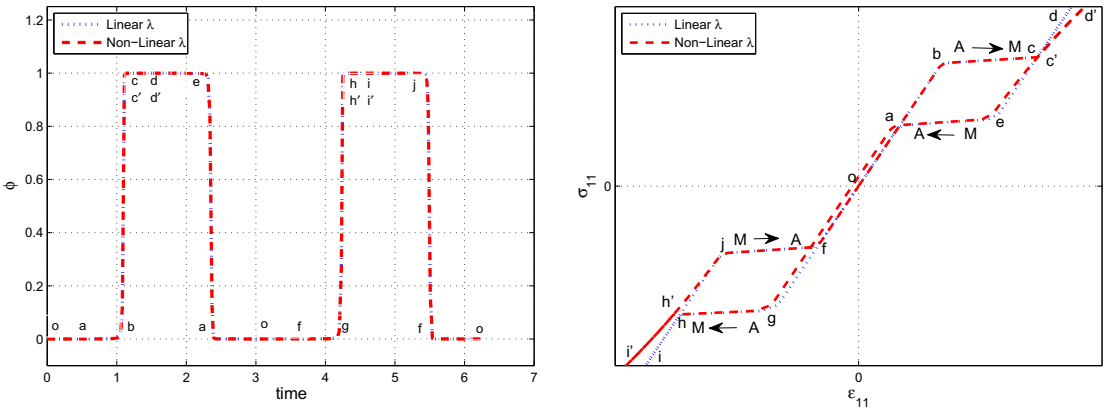

(a) ϕ vs time (b) $\sigma_{11} - \epsilon_{11}$curve

Fig. 8. Material response of a quasi-2D specimen at $\theta(8.5) > \theta_A(3)$.

$$\gamma\frac{\partial\phi}{\partial t}=\kappa\frac{\partial^2\phi}{\partial x^2}-\theta_0\frac{\partial}{\partial\phi}F(\phi)-[\hat{\theta}-\epsilon_0\cdot\boldsymbol{\sigma}]\frac{\partial}{\partial\phi}G(\phi). \tag{37}$$

By using the definitions of stress and strain tensors given by Eqs. (33)–(37) can now be simplified and solved for $\phi, B(t)$, and $g_1(t)$.

The simulations have been carried out with the dimensionless material parameters as follows:

$$\gamma=\frac{1}{100},\quad \kappa=0,\quad \theta_0=1,\quad \theta_A=3,\quad \epsilon_0=30,\quad \sigma_1=10,\quad \beta=\frac{1}{1000},\quad E=1,\quad A=1,\quad \theta=8.5,\quad \vartheta=0,\quad k=1,\quad \text{and}\quad \theta=8.5.$$

The compliance tensor coefficients for the linear λ case are $\lambda_2=E, \lambda_3=0$ and $\lambda_4=0$, and for the nonlinear λ case are $\lambda_2=E+\frac{1}{100}E\phi^2, \lambda_3=0$, and $\lambda_4=\frac{1}{100}E\phi^4$.

The phase evolution and σ_{11}–ϵ_{11} properties are shown in Fig. 8(a) and (b), respectively. It is observed that the σ_{11}–ϵ_{11} curve produces the pseudoelastic response. The hysteresis loop followed during the harmonic loading is represented by the path o-a-b-c-d-e-a-o-f-g-h-i-j-f-o for the linear λ case and by the path o-a-b-c′-d′-e-a-o-f-g-h′-i′-j-f-o for the nonlinear λ case, respectively. Fig. 9(a) and (b) show the σ_{22}–ϵ_{22} properties and evolution of strain components with time.

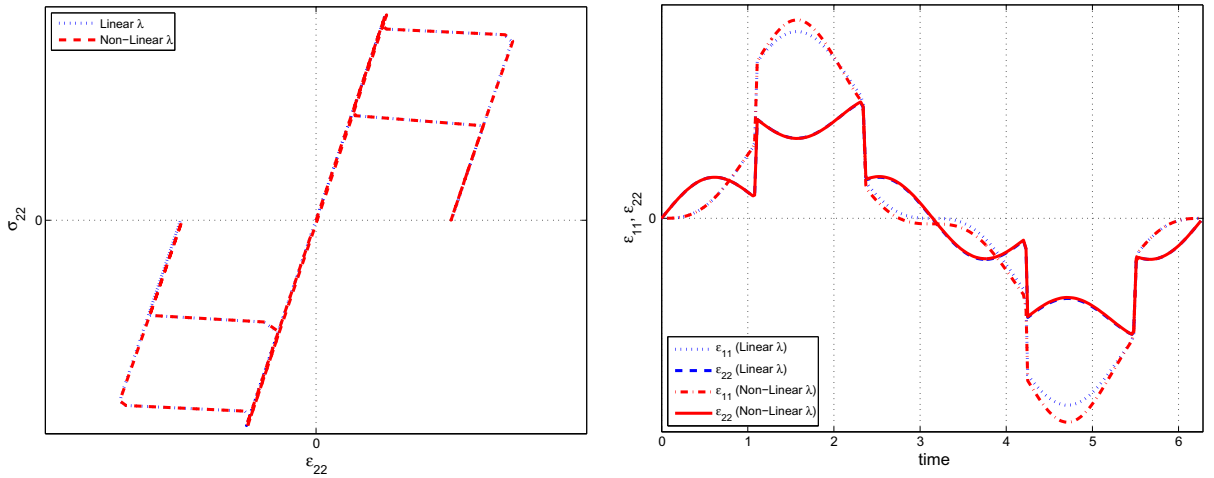

(a) σ_{22} vs ϵ_{22} Curve (b) $\epsilon_{11}, \epsilon_{22}$ vs time

Fig. 9. Material response of a quasi-2D specimen at $\theta(8.5) > \theta_A(3)$.

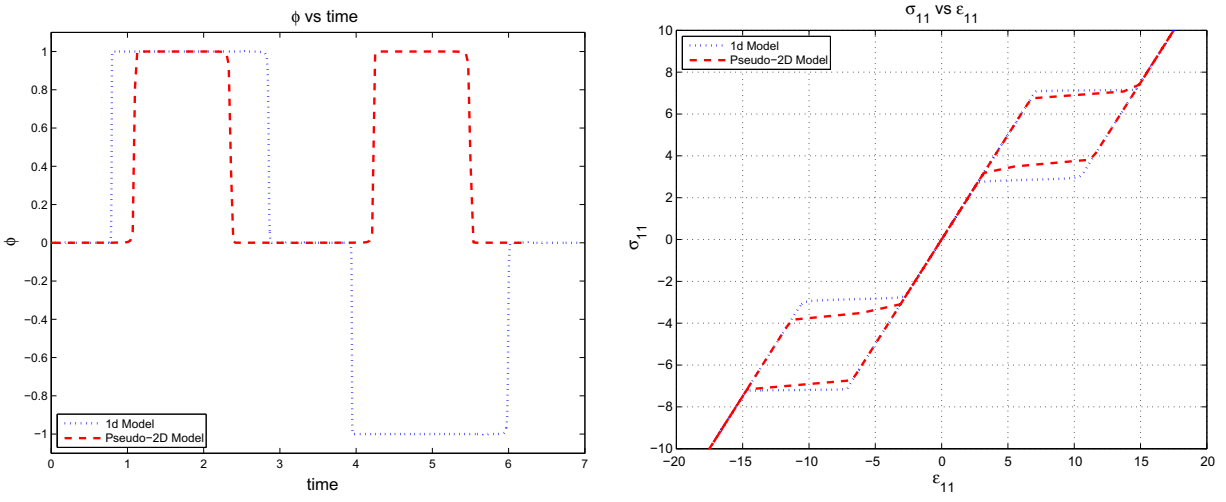

(a) ϕ vs time (b) $\sigma-\epsilon$ curve

Fig. 10. Comparison of one dimensional model results with the quasi-2D results.

We now compare the results based on the one dimensional model from Section 2.1 with the results obtained with the pseudo-2D model from Section 3.2.2. The results of one dimensional simulations (using equations given in the Section 2) have been obtained with the following coefficients:

$$\gamma = \frac{1}{100}, \quad \kappa = 0, \quad \theta_0 = 1, \quad \theta_M = 2, \quad \theta_A = 3, \quad \epsilon_0 = 30, \quad \beta = \frac{1}{1000}, \quad E = 1, \quad \alpha = 1, \quad \text{and} \quad \theta = 6.4.$$

Fig. 10(a) and (b) show the phase evolution and stress–strain plot for the linear λ case. We observe that the stress–strain curve qualitatively matches with the one dimensional results.

4. Conclusions

New non-isothermal thermodynamic models of SMA dynamics have been developed for the one-dimensional and generalized three dimensional case. An intrinsic feature of the developed models is their ability to account for nonlinear thermomechanical material properties via the compliance variable as the function of local phase and stress state. The models capture the SMA properties by coupling the phase evolution equation with the conservation laws of momentum and energy. They allow simple and efficient implementations. The model developed for the one dimensional case can deal with two distinct martensitic variants, and the nonlinear material properties are accounted for in this model via the phase and stress state and the corresponding compliance variable. The numerical simulations have been carried out, in the absence of gradient energy, to study such nonlinear material properties for all most important practical cases under stress induced loading. It has been observed that the stiffness of the stress–strain curve is reduced for the martensitic variants, which is in agreement with the experimental results. The three dimensional model has been developed with a scalar order parameter and rate dependent constitutive equations. The model describes the phase transformation using one order parameter at the expense of description of martensitic variants individually. It has been shown that the model is consistent with thermodynamics laws. Numerical simulations with this model have been carried out for quasi-2D specimens and the results have shown qualitative agreement with the results obtained with the one dimensional model.

The developed models can be applied to higher dimensional cases, as well as to the analysis of hysteresis phenomena coming from other application areas. This analysis is currently underway, and the results will be published elsewhere.

Acknowledgments

The authors thank Dr. Diego Grandi for providing useful insight into material parameter values. RD and RM have been supported by NSERC and CRC program, Canada, and JZ by NSERC. RM also acknowledges the hospitality and support of the Institute of Advanced Studies in Bologna, Italy.

References

[1] Bhattacharya K. Microstructure of martensite: Why it forms and how it gives rise to the shape-memory effect. Oxford University Press; 2003.
[2] Lagoudas D. Shape memory alloys: Modeling and engineering applications. London: Springer; 2008.
[3] Otsuka K, Wayman C. Shape memory materials. New York: Cambridge University Press; 1998.
[4] Melnik R, Roberts A, Thomas KA. Computing dynamics of copper-based SMA via center manifold reduction models. Comput Mater Sci 2002;18:255–68.
[5] Melnik R, Roberts A, Thomas KA. Phase transitions in shape memory alloys with hyperbolic heat conduction and differential-algebraic models. Comput Mech 2002;29(1):16–26.
[6] Melnik R, Roberts A. Modelling nonlinear dynamics of shape-memory-alloys with approximate models of coupled thermoelasticity. Z Angew Math Mech 2003;83(2):93–104.
[7] Wang L, Melnik R. Thermomechanical waves in SMA patches under small mechanical loadings. Lecture Notes in Comput Sci 2004;3029:645–52.
[8] Wang L, Melnik R. Mechanically induced phase combination in shape memory alloys by Chebyshev collocation methods. Mater Sci Eng A Struct Mater 2006;438–440:427–30.
[9] Wang L, Melnik R. Modifying macroscale variant combinations in a two-dimensional structure using mechanical loadings during thermally induced transformation. Mater Sci Eng A Struct Mater 2008;481–482:190–3.
[10] Wang L, Melnik R. Simulation of phase combinations in shape memory alloys patches by hybrid optimization methods. Appl Numer Math 2008;58(4):511–24.
[11] Khandelwal A, Buravalla V. Models for shape memory alloy behavior: An overview of modelling approaches. Int J Struct Changes Solids–Mech Appl 2009;1(1):111–48.
[12] Melnik R, Tsvilyuk O, Wang L. Low dimensional nonlinear thermomechanical models describing phase transformations and their applications. Rec. Adv. in Appl. Math. 2009:83–8 [Proceedings of the 14th WSEAS International Conference on Applied Mathematics].
[13] Melnik R, Wang L, Tsviliuk O. Phase transformations and shape memory effects in finite length nanostructures. Proc. of SPIE, Behavior and Mechanics of Multifunctional Materials and Composites 2010; 7644:1–10.
[14] Gao X, Huang M, Brinson L. A multivariant micromechanical model for SMAs Part 1. Crystallographic issues for single crystal model. Int J Plasticity 2000;16:1345–69.
[15] Huang M, Gao X, Brinson L. A multivariant micromechanical model for SMAs Part 2. Polycrystal model. Int J Plasticity 2000;16:1371–90.
[16] Lagoudas D, Brinson L, Patoor E. Shape memory alloys, part II: Modeling of polycrystals. Mech Mater 2006;38(5–6):430–62.
[17] Levitas V, Preston D. Three-dimensional Landau theory for multivariant stress-induced martensitic phase transformations. I. austenite ↔ martensite. Phys Rev B 2002;66(134206):1–9.
[18] Levitas V, Preston D. Three-dimensional Landau theory for multivariant stress-induced martensitic phase transformations. II. Multivariant phase transformations and stress space analysis. Phys Rev B 2002;66(134206):1–15.
[19] Levitas V, Preston D, Lee D. Three-dimensional Landau theory for multivariant stress-induced martensitic phase transformations. III. Alternative potentials, critical nuclei, kink solutions, and dislocation theory. Phys Rev B 2003;68(134201):1–24.
[20] Salje E. Phase transitions in ferroelastic and co-elastic crystals. Cambridge: Cambridge University Press; 1991.

[21] Toledano J, Toledano P. The Landau theory of phase transitions: Applications to structural, incommensurate, magnetic and liquid crystal systems, World Scientific, Singapore; 1987.
[22] Jacobs AE. Landau theory of a constrained ferroelastic in two dimensions. Phys Rev B Condens Matter 1995;52(9):6327–31.
[23] Lookman T, Shenoy SR, Rasmussen K, Saxena A, Bishop AR. Ferroelastic dynamics and strain compatibility. Phys Rev B Condens Matter Mater Phys 2003;67(2):24114.
[24] Bouville M, Ahluwalia R. Microstructure and mechanical properties of constrained shape memory alloy nanograins and nanowires. Acta Mater 2008;56(14):3558–67.
[25] Ahluwalia R, Lookman T, Saxena A. Dynamic strain loading of cubic to tetragonal martensites. MRS Bull 2006;54:2109–20.
[26] Grandi D, Maraldi M, Molari L. A macroscale phase-field model for shape memory alloys with non-isothermal effects: Influence of strain rate and environmental conditions on the mechanical response. Acta Mater 2012;60(1):179–91.
[27] Maraldi M, Molari L, Grandi D. A non-isothermal phase-field model for shape memory alloys: Numerical simulations of superelasticity and shape memory effect under stress-controlled conditions. J Intel Mat Syst Str 2012;23(10):1083–92.
[28] Dhote R, Melnik R, Zu J. Dynamic thermo-mechanical coupling and size effects in finite shape memory alloy nanostructures. Comput Mater Sci 2012;63:105–17.
[29] Berti V, Fabrizio M, Grandi D. Phase transitions in shape memory alloys: A non-isothermal Ginzburg Landau model. Phys D Nonlinear Phenom 2010;239(1–2):95–102.
[30] Falk F. Model free energy, mechanics, and thermodynamics of shape memory alloys. Acta Metall Mater 1980;28(12):1773–80.
[31] Wang Y, Khachaturyan A. Three-dimensional field model and computer modeling of martensitic transformations. Acta Mater 1997;45(2):759–73.
[32] Curnoe S, Jacobs A. Twin wall of proper cubic-tetragonal ferroelastics. Phys Rev B 2000;62(18):11925–8.
[33] Bouville M, Ahluwalia R. Phase field simulations of coupled phase transformations in ferroelastic–ferroelastic nanocomposites. Phys Rev B 2009;79(9):094110.
[34] Mahapatra D, Melnik R. Finite element analysis of phase transformation dynamics in shape memory alloys with a consistent Landau-Ginzburg free energy model. Mech Adv Mater Struct 2006;13:443–55.
[35] Mahapatra D, Melnik R. Finite element approach to modelling evolution of 3D shape memory materials. Math Comput Simulat 2007;76:141–8.
[36] Lloveras P, Castán T, Porta M, Planes A, Saxena A. Thermodynamics of stress-induced ferroelastic transitions: Influence of anisotropy and disorder. Phys Rev B 2010;81(21):214105.
[37] Levitas V, Lee D. Athermal resistance to interface motion in the phase-field theory of microstructure evolution. Phys Rev Lett 2007;99(24):245701.
[38] Levitas V, Lee D, Preston D. Interface propagation and microstructure evolution in phase field models of stress-induced martensitic phase transformations. Int J Plasticity 2010;26(3):395–422.
[39] Berti V, Fabrizio M, Grandi D. Hysteresis and phase transitions for one-dimensional and three-dimensional models in shape memory alloys. J Math Phys 2010;51(6):062901.
[40] Fabrizio M. Ice-water and liquid-vapor phase transitions by a Ginzburg–Landau model. J Math Phys 2008;49:102902.
[41] Fabrizio M, Giorgi C, Morro A. A continuum theory for first order phase transitions based on the balance of structure order. Method Appl Sci 2008;31(6):627–53.
[42] Christ D, Reese S. A finite element model for shape memory alloys considering thermomechanical couplings at large strains. Int J Solids Struct 2009;46(20):3694–709.
[43] Song J, Ahluwalia R. Critical size for phase separation in binary alloys: Role of elastic interactions and mechanical constraints. Phys Rev B 2008;78(6):064204.
[44] Matus P, Melnik RVN, Wang L, Rybak I. Applications of fully conservative schemes in nonlinear thermoelasticity: Modelling shape memory materials. Math Comput Simulat 2004;65(4–5):489–509.
[45] Wang L, Melnik R. Model reduction applied to square to rectangular martensitic transformations using proper orthogonal decomposition. Appl Numer Math 2007;57(5):510–20.
[46] Wang L, Melnik R. Finite volume analysis of nonlinear thermo-mechanical dynamics of shape memory alloys. Heat Mass Tran. 2007;43:535–46.